

Measurement of branching ratio and B_s^0 lifetime in the decay $B_s^0 \rightarrow J/\psi f_0(980)$ at CDF

T. Aaltonen,²¹ B. Álvarez González^{w,9} S. Amerio,⁴¹ D. Amidei,³² A. Anastassov,³⁶ A. Annovi,¹⁷ J. Antos,¹² G. Apollinari,¹⁵ J.A. Appel,¹⁵ A. Apresyan,⁴⁶ T. Arisawa,⁵⁶ A. Artikov,¹³ J. Asaadi,⁵¹ W. Ashmanskas,¹⁵ B. Auerbach,⁵⁹ A. Aurisano,⁵¹ F. Azfar,⁴⁰ W. Badgett,¹⁵ A. Barbaro-Galtieri,²⁶ V.E. Barnes,⁴⁶ B.A. Barnett,²³ P. Barria^{dd,44} P. Bartos,¹² M. Bauce^{bb,41} G. Bauer,³⁰ F. Bedeschi,⁴⁴ D. Beecher,²⁸ S. Behari,²³ G. Bellettini^{cc,44} J. Bellinger,⁵⁸ D. Benjamin,¹⁴ A. Beretvas,¹⁵ A. Bhatti,⁴⁸ M. Binkley^{*},¹⁵ D. Bisello^{bb,41} I. Bizjak^{hh,28} K.R. Bland,⁵ B. Blumenfeld,²³ A. Bocci,¹⁴ A. Bodek,⁴⁷ D. Bortoletto,⁴⁶ J. Boudreau,⁴⁵ A. Boveia,¹¹ B. Brau^{a,15} L. Brigliadori^{aa,6} A. Brisuda,¹² C. Bromberg,³³ E. Brucken,²¹ M. Bucciantonio^{cc,44} J. Budagov,¹³ H.S. Budd,⁴⁷ S. Budd,²² K. Burkett,¹⁵ G. Busetto^{bb,41} P. Bussey,¹⁹ A. Buzatu,³¹ C. Calancha,²⁹ S. Camarda,⁴ M. Campanelli,³³ M. Campbell,³² F. Canelli^{11,15} B. Carls,²² D. Carlsmith,⁵⁸ R. Carosi,⁴⁴ S. Carrillo^{k,16} S. Carron,¹⁵ B. Casal,⁹ M. Casarsa,¹⁵ A. Castro^{aa,6} P. Catastini,²⁰ D. Cauz,⁵² V. Cavaliere,²² M. Cavalli-Sforza,⁴ A. Cerri^{f,26} L. Cerrito^{q,28} Y.C. Chen,¹ M. Chertok,⁷ G. Chiarelli,⁴⁴ G. Chlachidze,¹⁵ F. Chlebana,¹⁵ K. Cho,²⁵ D. Chokheli,¹³ J.P. Chou,²⁰ W.H. Chung,⁵⁸ Y.S. Chung,⁴⁷ C.I. Ciobanu,⁴² M.A. Ciocci^{dd,44} A. Clark,¹⁸ C. Clarke,⁵⁷ G. Compostella^{bb,41} M.E. Convery,¹⁵ J. Conway,⁷ M. Corbo,⁴² M. Cordelli,¹⁷ C.A. Cox,⁷ D.J. Cox,⁷ F. Crescioli^{cc,44} C. Cuenca Almenar,⁵⁹ J. Cuevas^{w,9} R. Culbertson,¹⁵ D. Dagenhart,¹⁵ N. d'Ascenzo^{u,42} M. Datta,¹⁵ P. de Barbaro,⁴⁷ S. De Cecco,⁴⁹ G. De Lorenzo,⁴ M. Dell'Orso^{cc,44} C. Deluca,⁴ L. Demortier,⁴⁸ J. Deng^{c,14} M. Deninno,⁶ F. Devoto,²¹ M. d'Errico^{bb,41} A. Di Canto^{cc,44} B. Di Ruzza,⁴⁴ J.R. Dittmann,⁵ M. D'Onofrio,²⁷ S. Donati^{cc,44} P. Dong,¹⁵ M. Dorigo,⁵² T. Dorigo,⁴¹ K. Ebina,⁵⁶ A. Elagin,⁵¹ A. Eppig,³² R. Erbacher,⁷ D. Errede,²² S. Errede,²² N. Ershaidat^{z,42} R. Eusebi,⁵¹ H.C. Fang,²⁶ S. Farrington,⁴⁰ M. Feindt,²⁴ J.P. Fernandez,²⁹ C. Ferrazza^{ee,44} R. Field,¹⁶ G. Flanagan^{s,46} R. Forrest,⁷ M.J. Frank,⁵ M. Franklin,²⁰ J.C. Freeman,¹⁵ Y. Funakoshi,⁵⁶ I. Furic,¹⁶ M. Gallinaro,⁴⁸ J. Galyardt,¹⁰ J.E. Garcia,¹⁸ A.F. Garfinkel,⁴⁶ P. Garosi^{dd,44} H. Gerberich,²² E. Gerchtein,¹⁵ S. Giagu^{ff,49} V. Giakoumopoulou,³ P. Giannetti,⁴⁴ K. Gibson,⁴⁵ C.M. Ginsburg,¹⁵ N. Giokaris,³ P. Giromini,¹⁷ M. Giunta,⁴⁴ G. Giurgiu,²³ V. Glagolev,¹³ D. Glenzinski,¹⁵ M. Gold,³⁵ D. Goldin,⁵¹ N. Goldschmidt,¹⁶ A. Golossanov,¹⁵ G. Gomez,⁹ G. Gomez-Ceballos,³⁰ M. Goncharov,³⁰ O. González,²⁹ I. Gorelov,³⁵ A.T. Goshaw,¹⁴ K. Goulianos,⁴⁸ S. Grinstein,⁴ C. Grosso-Pilcher,¹¹ R.C. Group^{55,15} J. Guimaraes da Costa,²⁰ Z. Gunay-Unalan,³³ C. Haber,²⁶ S.R. Hahn,¹⁵ E. Halkiadakis,⁵⁰ A. Hamaguchi,³⁹ J.Y. Han,⁴⁷ F. Happacher,¹⁷ K. Hara,⁵³ D. Hare,⁵⁰ M. Hare,⁵⁴ R.F. Harr,⁵⁷ K. Hatakeyama,⁵ C. Hays,⁴⁰ M. Heck,²⁴ J. Heinrich,⁴³ M. Herndon,⁵⁸ S. Hewamanage,⁵ D. Hidas,⁵⁰ A. Hocker,¹⁵ W. Hopkins^{g,15} D. Horn,²⁴ S. Hou,¹ R.E. Hughes,³⁷ M. Hurwitz,¹¹ M. Huschle,²⁴ U. Husemann,⁵⁹ N. Hussain,³¹ M. Hussein,³³ J. Huston,³³ G. Introzzi,⁴⁴ M. Iori^{ff,49} A. Ivanov^{o,7} E. James,¹⁵ D. Jang,¹⁰ B. Jayatilaka,¹⁴ E.J. Jeon,²⁵ M.K. Jha,⁶ S. Jindariani,¹⁵ W. Johnson,⁷ M. Jones,⁴⁶ K.K. Joo,²⁵ S.Y. Jun,¹⁰ T.R. Junk,¹⁵ T. Kamon,⁵¹ P.E. Karchin,⁵⁷ A. Kasmai,⁵ Y. Kato^{n,39} W. Ketchum,¹¹ J. Keung,⁴³ V. Khotilovich,⁵¹ B. Kilminster,¹⁵ D.H. Kim,²⁵ H.S. Kim,²⁵ H.W. Kim,²⁵ J.E. Kim,²⁵ M.J. Kim,¹⁷ S.B. Kim,²⁵ S.H. Kim,⁵³ Y.K. Kim,¹¹ N. Kimura,⁵⁶ M. Kirby,¹⁵ S. Klimenko,¹⁶ K. Kondo,⁵⁶ D.J. Kong,²⁵ J. Konigsberg,¹⁶ A.V. Kotwal,¹⁴ M. Kreps^{ii,24} J. Kroll,⁴³ D. Krop,¹¹ N. Krumnack^{l,5} M. Kruse,¹⁴ V. Krutelyov^{d,51} T. Kuhr,²⁴ M. Kurata,⁵³ S. Kwang,¹¹ A.T. Laasanen,⁴⁶ S. Lami,⁴⁴ S. Lammel,¹⁵ M. Lancaster,²⁸ R.L. Lander,⁷ K. Lannon^{v,37} A. Lath,⁵⁰ G. Latino^{cc,44} T. LeCompte,² E. Lee,⁵¹ H.S. Lee,¹¹ J.S. Lee,²⁵ S.W. Lee^{x,51} S. Leo^{cc,44} S. Leone,⁴⁴ J.D. Lewis,¹⁵ A. Limosani^{r,14} C.-J. Lin,²⁶ J. Linacre,⁴⁰ M. Lindgren,¹⁵ E. Lipeles,⁴³ A. Lister,¹⁸ D.O. Litvintsev,¹⁵ C. Liu,⁴⁵ Q. Liu,⁴⁶ T. Liu,¹⁵ S. Lockwitz,⁵⁹ A. Loginov,⁵⁹ D. Lucchesi^{bb,41} J. Lueck,²⁴ P. Lujan,²⁶ P. Lukens,¹⁵ G. Lungu,⁴⁸ J. Lys,²⁶ R. Lysak,¹² R. Madrak,¹⁵ K. Maeshima,¹⁵ K. Makhoul,³⁰ S. Malik,⁴⁸ G. Manca^{b,27} A. Manousakis-Katsikakis,³ F. Margaroli,⁴⁶ C. Marino,²⁴ M. Martínez,⁴ R. Martínez-Ballarín,²⁹ P. Mastrandrea,⁴⁹ M.E. Mattson,⁵⁷ P. Mazzanti,⁶ K.S. McFarland,⁴⁷ P. McIntyre,⁵¹ R. McNulty^{i,27} A. Mehta,²⁷ P. Mehtala,²¹ A. Menzione,⁴⁴ C. Mesropian,⁴⁸ T. Miao,¹⁵ D. Mietlicki,³² A. Mitra,¹ H. Miyake,⁵³ S. Moed,²⁰ N. Moggi,⁶ M.N. Mondragon^{k,15} C.S. Moon,²⁵ R. Moore,¹⁵ M.J. Morello,¹⁵ J. Morlock,²⁴ P. Movilla Fernandez,¹⁵ A. Mukherjee,¹⁵ Th. Muller,²⁴ P. Murat,¹⁵ M. Mussini^{aa,6} J. Nachtman^{m,15} Y. Nagai,⁵³ J. Naganoma,⁵⁶ I. Nakano,³⁸ A. Napier,⁵⁴ J. Nett,⁵¹ C. Neu,⁶⁰ M.S. Neubauer,²² J. Nielsen^{e,26} L. Nodulman,² O. Norriella,²² E. Nurse,²⁸ L. Oakes,⁴⁰ S.H. Oh,¹⁴ Y.D. Oh,²⁵ I. Oksuzian,⁶⁰ T. Okusawa,³⁹ R. Orava,²¹ L. Ortolan,⁴ S. Pagan Griso^{bb,41} C. Pagliarone,⁵² E. Palencia^{f,9} V. Papadimitriou,¹⁵ A.A. Paramonov,² J. Patrick,¹⁵ G. Pauletta^{gg,52} M. Paulini,¹⁰ C. Paus,³⁰ D.E. Pellett,⁷ A. Penzo,⁵² T.J. Phillips,¹⁴ G. Piacentino,⁴⁴ E. Pianori,⁴³ J. Pilot,³⁷ K. Pitts,²² C. Plager,⁸ L. Pondrom,⁵⁸ K. Potamianos,⁴⁶ O. Poukhov^{*},¹³ F. Prokoshin^{y,13} A. Pronko,¹⁵ F. Ptohos^{h,17} E. Pueschel,¹⁰ G. Punzi^{cc,44} J. Pursley,⁵⁸ A. Rahaman,⁴⁵ V. Ramakrishnan,⁵⁸ N. Ranjan,⁴⁶ I. Redondo,²⁹ P. Renton,⁴⁰ M. Rescigno,⁴⁹ T. Riddick,²⁸ F. Rimondi^{aa,6} L. Ristori^{44,15} A. Robson,¹⁹ T. Rodrigo,⁹ T. Rodriguez,⁴³ E. Rogers,²² S. Rolli,⁵⁴ R. Roser,¹⁵ M. Rossi,⁵² F. Rubbo,¹⁵ F. Ruffini^{dd,44} A. Ruiz,⁹ J. Russ,¹⁰ V. Rusu,¹⁵ A. Safonov,⁵¹ W.K. Sakumoto,⁴⁷ Y. Sakurai,⁵⁶ L. Santi^{gg,52} L. Sartori,⁴⁴

K. Sato,⁵³ V. Saveliev^{u,42} A. Savoy-Navarro,⁴² P. Schlabach,¹⁵ A. Schmidt,²⁴ E.E. Schmidt,¹⁵ M.P. Schmidt*,⁵⁹ M. Schmitt,³⁶ T. Schwarz,⁷ L. Scodellaro,⁹ A. Scribano^{ad,44} F. Scuri,⁴⁴ A. Sedov,⁴⁶ S. Seidel,³⁵ Y. Seiya,³⁹ A. Semenov,¹³ F. Sforza^{cc,44} A. Sfyrla,²² S.Z. Shalhout,⁷ T. Shears,²⁷ P.F. Shepard,⁴⁵ M. Shimojima^{t,53} S. Shiraishi,¹¹ M. Shochet,¹¹ I. Shreyber,³⁴ A. Simonenko,¹³ P. Sinervo,³¹ A. Sissakian*,¹³ K. Sliwa,⁵⁴ J.R. Smith,⁷ F.D. Snider,¹⁵ A. Soha,¹⁵ S. Somalwar,⁵⁰ V. Sorin,⁴ P. Squillacioti,¹⁵ M. Stancari,¹⁵ M. Stanitzki,⁵⁹ R. St. Denis,¹⁹ B. Stelzer,³¹ O. Stelzer-Chilton,³¹ D. Stentz,³⁶ J. Strologas,³⁵ G.L. Strycker,³² Y. Sudo,⁵³ A. Sukhanov,¹⁶ I. Suslov,¹³ K. Takemasa,⁵³ Y. Takeuchi,⁵³ J. Tang,¹¹ M. Tecchio,³² P.K. Teng,¹ J. Thom^{g,15} J. Thome,¹⁰ G.A. Thompson,²² E. Thomson,⁴³ P. Ttito-Guzmán,²⁹ S. Tkaczyk,¹⁵ D. Toback,⁵¹ S. Tokar,¹² K. Tollefson,³³ T. Tomura,⁵³ D. Tonelli,¹⁵ S. Torre,¹⁷ D. Torretta,¹⁵ P. Totaro,⁴¹ M. Trovato^{ce,44} Y. Tu,⁴³ F. Ukegawa,⁵³ S. Uozumi,²⁵ A. Varganov,³² F. Vázquez^{k,16} G. Velez,¹⁵ C. Vellidis,³ M. Vidal,²⁹ I. Vila,⁹ R. Vilar,⁹ J. Vizán,⁹ M. Vogel,³⁵ G. Volpi^{cc,44} P. Wagner,⁴³ R.L. Wagner,¹⁵ T. Wakisaka,³⁹ R. Wallny,⁸ S.M. Wang,¹ A. Warburton,³¹ D. Waters,²⁸ M. Weinberger,⁵¹ W.C. Wester III,¹⁵ B. Whitehouse,⁵⁴ D. Whiteson^{c,43} A.B. Wicklund,² E. Wicklund,¹⁵ S. Wilbur,¹¹ F. Wick,²⁴ H.H. Williams,⁴³ J.S. Wilson,³⁷ P. Wilson,¹⁵ B.L. Winer,³⁷ P. Wittich^{g,15} S. Wolbers,¹⁵ H. Wolfe,³⁷ T. Wright,³² X. Wu,¹⁸ Z. Wu,⁵ K. Yamamoto,³⁹ J. Yamaoka,¹⁴ T. Yang,¹⁵ U.K. Yang^{p,11} Y.C. Yang,²⁵ W.-M. Yao,²⁶ G.P. Yeh,¹⁵ K. Yi^{m,15} J. Yoh,¹⁵ K. Yorita,⁵⁶ T. Yoshida^{j,39} G.B. Yu,¹⁴ I. Yu,²⁵ S.S. Yu,¹⁵ J.C. Yun,¹⁵ A. Zanetti,⁵² Y. Zeng,¹⁴ and S. Zucchelli^{aa6}
(CDF Collaboration[†])

¹*Institute of Physics, Academia Sinica, Taipei, Taiwan 11529, Republic of China*

²*Argonne National Laboratory, Argonne, Illinois 60439, USA*

³*University of Athens, 157 71 Athens, Greece*

⁴*Institut de Física d'Altes Energies, ICREA, Universitat Autònoma de Barcelona, E-08193, Bellaterra (Barcelona), Spain*

⁵*Baylor University, Waco, Texas 76798, USA*

⁶*Istituto Nazionale di Fisica Nucleare Bologna, ^{aa}University of Bologna, I-40127 Bologna, Italy*

⁷*University of California, Davis, Davis, California 95616, USA*

⁸*University of California, Los Angeles, Los Angeles, California 90024, USA*

⁹*Instituto de Física de Cantabria, CSIC-University of Cantabria, 39005 Santander, Spain*

¹⁰*Carnegie Mellon University, Pittsburgh, Pennsylvania 15213, USA*

¹¹*Enrico Fermi Institute, University of Chicago, Chicago, Illinois 60637, USA*

¹²*Comenius University, 842 48 Bratislava, Slovakia; Institute of Experimental Physics, 040 01 Kosice, Slovakia*

¹³*Joint Institute for Nuclear Research, RU-141980 Dubna, Russia*

¹⁴*Duke University, Durham, North Carolina 27708, USA*

¹⁵*Fermi National Accelerator Laboratory, Batavia, Illinois 60510, USA*

¹⁶*University of Florida, Gainesville, Florida 32611, USA*

¹⁷*Laboratori Nazionali di Frascati, Istituto Nazionale di Fisica Nucleare, I-00044 Frascati, Italy*

¹⁸*University of Geneva, CH-1211 Geneva 4, Switzerland*

¹⁹*Glasgow University, Glasgow G12 8QQ, United Kingdom*

²⁰*Harvard University, Cambridge, Massachusetts 02138, USA*

²¹*Division of High Energy Physics, Department of Physics, University of Helsinki and Helsinki Institute of Physics, FIN-00014, Helsinki, Finland*

²²*University of Illinois, Urbana, Illinois 61801, USA*

²³*The Johns Hopkins University, Baltimore, Maryland 21218, USA*

²⁴*Institut für Experimentelle Kernphysik, Karlsruhe Institute of Technology, D-76131 Karlsruhe, Germany*

²⁵*Center for High Energy Physics: Kyungpook National University,*

Daegu 702-701, Korea; Seoul National University, Seoul 151-742,

Korea; Sungkyunkwan University, Suwon 440-746,

Korea; Korea Institute of Science and Technology Information,

Daejeon 305-806, Korea; Chonnam National University, Gwangju 500-757,

Korea; Chonbuk National University, Jeonju 561-756, Korea

²⁶*Ernest Orlando Lawrence Berkeley National Laboratory, Berkeley, California 94720, USA*

²⁷*University of Liverpool, Liverpool L69 7ZE, United Kingdom*

²⁸*University College London, London WC1E 6BT, United Kingdom*

²⁹*Centro de Investigaciones Energéticas Medioambientales y Tecnológicas, E-28040 Madrid, Spain*

³⁰*Massachusetts Institute of Technology, Cambridge, Massachusetts 02139, USA*

³¹*Institute of Particle Physics: McGill University, Montréal, Québec,*

Canada H3A 2T8; Simon Fraser University, Burnaby, British Columbia,

Canada V5A 1S6; University of Toronto, Toronto, Ontario,

Canada M5S 1A7; and TRIUMF, Vancouver, British Columbia, Canada V6T 2A3

³²*University of Michigan, Ann Arbor, Michigan 48109, USA*

³³*Michigan State University, East Lansing, Michigan 48824, USA*

³⁴*Institution for Theoretical and Experimental Physics, ITEP, Moscow 117259, Russia*

- ³⁵University of New Mexico, Albuquerque, New Mexico 87131, USA
³⁶Northwestern University, Evanston, Illinois 60208, USA
³⁷The Ohio State University, Columbus, Ohio 43210, USA
³⁸Okayama University, Okayama 700-8530, Japan
³⁹Osaka City University, Osaka 588, Japan
⁴⁰University of Oxford, Oxford OX1 3RH, United Kingdom
⁴¹Istituto Nazionale di Fisica Nucleare, Sezione di Padova-Trento, ^{bb}University of Padova, I-35131 Padova, Italy
⁴²LPNHE, Universite Pierre et Marie Curie/IN2P3-CNRS, UMR7585, Paris, F-75252 France
⁴³University of Pennsylvania, Philadelphia, Pennsylvania 19104, USA
⁴⁴Istituto Nazionale di Fisica Nucleare Pisa, ^{cc}University of Pisa,
^{dd}University of Siena and ^{ee}Scuola Normale Superiore, I-56127 Pisa, Italy
⁴⁵University of Pittsburgh, Pittsburgh, Pennsylvania 15260, USA
⁴⁶Purdue University, West Lafayette, Indiana 47907, USA
⁴⁷University of Rochester, Rochester, New York 14627, USA
⁴⁸The Rockefeller University, New York, New York 10065, USA
⁴⁹Istituto Nazionale di Fisica Nucleare, Sezione di Roma 1,
^{ff}Sapienza Università di Roma, I-00185 Roma, Italy
⁵⁰Rutgers University, Piscataway, New Jersey 08855, USA
⁵¹Texas A&M University, College Station, Texas 77843, USA
⁵²Istituto Nazionale di Fisica Nucleare Trieste/Udine,
I-34100 Trieste, ^{gg}University of Udine, I-33100 Udine, Italy
⁵³University of Tsukuba, Tsukuba, Ibaraki 305, Japan
⁵⁴Tufts University, Medford, Massachusetts 02155, USA
⁵⁵University of Virginia, Charlottesville, Virginia 22906, USA
⁵⁶Waseda University, Tokyo 169, Japan
⁵⁷Wayne State University, Detroit, Michigan 48201, USA
⁵⁸University of Wisconsin, Madison, Wisconsin 53706, USA
⁵⁹Yale University, New Haven, Connecticut 06520, USA
⁶⁰University of Virginia, Charlottesville, VA 22906, USA

We present a study of B_s^0 decays to the CP -odd final state $J/\psi f_0(980)$ with $J/\psi \rightarrow \mu^+ \mu^-$ and $f_0(980) \rightarrow \pi^+ \pi^-$. Using $p\bar{p}$ collision data with an integrated luminosity of 3.8 fb^{-1} collected by the CDF II detector at the Tevatron we measure a B_s^0 lifetime of $\tau(B_s^0 \rightarrow J/\psi f_0(980)) = 1.70_{-0.11}^{+0.12}(\text{stat}) \pm 0.03(\text{syst}) \text{ ps}$. This is the first measurement of the B_s^0 lifetime in a decay to a CP eigenstate and corresponds in the standard model to the lifetime of the heavy B_s^0 eigenstate. We also measure the product of branching fractions of $B_s^0 \rightarrow J/\psi f_0(980)$ and $f_0(980) \rightarrow \pi^+ \pi^-$ relative to the product of branching fractions of $B_s^0 \rightarrow J/\psi \phi$ and $\phi \rightarrow K^+ K^-$ to be $R_{f_0/\phi} = 0.257 \pm 0.020(\text{stat}) \pm 0.014(\text{syst})$, which is the most precise determination of this quantity to date.

PACS numbers: 13.25.Hw, 14.40.Nd, 12.15.Ff

I. INTRODUCTION

*Deceased

†With visitors from ^aUniversity of MA Amherst, Amherst, MA 01003, USA, ^bIstituto Nazionale di Fisica Nucleare, Sezione di Cagliari, 09042 Monserrato (Cagliari), Italy, ^cUniversity of CA Irvine, Irvine, CA 92697, USA, ^dUniversity of CA Santa Barbara, Santa Barbara, CA 93106, USA, ^eUniversity of CA Santa Cruz, Santa Cruz, CA 95064, USA, ^fCERN, CH-1211 Geneva, Switzerland, ^gCornell University, Ithaca, NY 14853, USA, ^hUniversity of Cyprus, Nicosia CY-1678, Cyprus, ⁱUniversity College Dublin, Dublin 4, Ireland, ^jUniversity of Fukui, Fukui City, Fukui Prefecture, Japan 910-0017, ^kUniversidad Iberoamericana, Mexico D.F., Mexico, ^lIowa State University, Ames, IA 50011, USA, ^mUniversity of Iowa, Iowa City, IA 52242, USA, ⁿKinki University, Higashi-Osaka City, Japan 577-8502, ^oKansas State University, Manhattan, KS 66506, USA, ^pUniversity of Manchester, Manchester M13 9PL, United Kingdom, ^qQueen Mary, University of London, London, E1 4NS, United Kingdom, ^rUniversity of Melbourne, Victoria 3010, Australia, ^sMuons, Inc., Batavia, IL 60510, USA, ^tNagasaki Institute of Applied Science, Nagasaki, Japan, ^uNational Research Nuclear University, Moscow, Russia, ^vUniversity of Notre Dame, Notre Dame, IN 46556, USA, ^wUniversidad de Oviedo, E-

In the standard model, the mass and flavor eigenstates of the B_s^0 meson are not identical. This gives rise to particle – anti-particle oscillations [1], which proceed in the standard model through second order weak interaction processes, and whose phenomenology depends on the Cabibbo-Kobayashi-Maskawa (CKM) quark mixing matrix. The time (t) evolution of B_s^0 mesons is approxi-

33007 Oviedo, Spain, ^xTexas Tech University, Lubbock, TX 79609, USA, ^yUniversidad Tecnica Federico Santa Maria, 110v Valparaiso, Chile, ^zYarmouk University, Irbid 211-63, Jordan, ^{hh}On leave from J. Stefan Institute, Ljubljana, Slovenia, ⁱⁱUniversity of Warwick, Coventry CV4 7AL, United Kingdom,

mately governed by the Schrödinger equation

$$i \frac{d}{dt} \begin{pmatrix} |B_s^0(t)\rangle \\ |\bar{B}_s^0(t)\rangle \end{pmatrix} = \left(\hat{M}^s - \frac{i}{2} \hat{\Gamma}^s \right) \begin{pmatrix} |B_s^0(t)\rangle \\ |\bar{B}_s^0(t)\rangle \end{pmatrix}, \quad (1)$$

where \hat{M}^s and $\hat{\Gamma}^s$ are mass and decay rate symmetric 2×2 matrices. Diagonalization of $\hat{M}^s - \frac{i}{2} \hat{\Gamma}^s$ leads to mass eigenstates

$$|B_{sL}^0\rangle = p |B_s^0\rangle + q |\bar{B}_s^0\rangle, \quad (2)$$

$$|B_{sH}^0\rangle = p |B_s^0\rangle - q |\bar{B}_s^0\rangle, \quad (3)$$

with distinct masses (M_s^L, M_s^H) and distinct decay rates (Γ_s^L, Γ_s^H), where p and q are complex numbers satisfying $|p|^2 + |q|^2 = 1$. An important feature of the B_s^0 system is the non-zero matrix element Γ_{12}^s representing the partial width of B_s^0 and \bar{B}_s^0 decays to common final states which translates into a non-zero decay width difference $\Delta\Gamma_s$ of the two mass eigenstates through the relation

$$\Delta\Gamma_s = \Gamma_s^L - \Gamma_s^H = 2|\Gamma_{12}^s| \cos\phi_s, \quad (4)$$

where $\phi_s = \arg(-M_{12}^s/\Gamma_{12}^s)$. The phase ϕ_s describes CP violation in B_s^0 mixing. In the standard model ϕ_s is predicted to be $0.22^\circ \pm 0.06^\circ$ [2, 3]. The small value of the phase ϕ_s causes the mass and CP eigenstates to coincide to a good approximation. Thus the measurement of the lifetime in a CP eigenstate provides directly the lifetime of the corresponding mass eigenstate. If new physics is present, it could enhance ϕ_s to large values, a scenario which is not excluded by current experimental constraints. In such a case the correspondence between mass and CP eigenstates does not hold anymore and the measured lifetime will correspond to the weighted average of the lifetimes of the two mass eigenstates with weights dependent on the size of the CP violating phase ϕ_s [4]. Thus a measurement of the B_s^0 lifetime in a final state which is a CP eigenstate provides, in combination with other measurements, valuable information on the decay width difference $\Delta\Gamma_s$ and the CP violation in B_s^0 mixing.

One of the most powerful measurements to constrain a new physics contribution to the phase ϕ_s is the measurement of CP violation in the decay $B_s^0 \rightarrow J/\psi\phi$ with $\phi \rightarrow K^+K^-$. The decay $B_s^0 \rightarrow J/\psi\phi$ has a mixture of the CP -even and -odd components in the final state and an angular analysis is needed to separate them [5]. In the standard model, CP violation in the decay $B_s^0 \rightarrow J/\psi\phi$ is given by $2\beta_s = \arg[(-V_{ts}V_{tb}^*)/(V_{cs}V_{cb}^*)]$. New physics effects would shift ϕ_s and $-2\beta_s$ from the standard model value by the same amount. A sufficiently copious $B_s^0 \rightarrow J/\psi f_0$ signal with $f_0 \rightarrow \pi^+\pi^-$, where f_0 stands for $f_0(980)$, and B_s^0 flavor identified at production can be used to measure β_s without the need of an angular analysis [6] as $J/\psi f_0$ is a pure CP -odd final state. Since the B_s^0 is a spin 0 particle and the decay products J/ψ and f_0 have quantum numbers $J^{PC} = 1^{--}$ and 0^{++} , respectively, the final state has an orbital angular momentum of $L = 1$ leading to a CP eigenvalue of

$(-1)^L = -1$. Further interest in the decay $B_s^0 \rightarrow J/\psi f_0$ arises from its possible contribution to an S -wave component in the $B_s^0 \rightarrow J/\psi K^+K^-$ decay if the f_0 decays to K^+K^- . This contribution could help to resolve an ambiguity in the $\Delta\Gamma_s$ and β_s values determined in the $B_s^0 \rightarrow J/\psi\phi$ analyses. Because it was neglected in the first tagged $B_s^0 \rightarrow J/\psi\phi$ results [7, 8], each of which showed an approximately 1.5σ deviation from the standard model, it was argued that the omission may significantly bias the results [9, 10]. However, using the formalism in Ref. [11], the latest preliminary CDF measurement [12] has shown that the S -wave interference effect is negligible at the current level of precision.

In Refs. [2, 3] the decay width difference in the standard model is predicted to be $\Delta\Gamma_s^{\text{SM}} = (0.087 \pm 0.021)$ ps^{-1} and the ratio of the average B_s^0 lifetime, $\tau_s = 2/(\Gamma_s^L + \Gamma_s^H)$, to the B^0 lifetime, τ_d , to be $0.996 < \tau_s/\tau_d < 1$. Using these predictions in the relations

$$\Gamma_s^H = \frac{1}{\tau_s^H} = \Gamma_s - \frac{1}{2}\Delta\Gamma_s, \quad (5)$$

$$\Gamma_s^L = \frac{1}{\tau_s^L} = \Gamma_s + \frac{1}{2}\Delta\Gamma_s, \quad (6)$$

where $\Gamma_s = 1/\tau_s$, together with the world average B^0 lifetime, $\tau_d = (1.525 \pm 0.009)$ ps [13], we find the theoretically-derived values $\tau_s^H = (1.630 \pm 0.030)$ ps and $\tau_s^L = (1.427 \pm 0.023)$ ps.

While no direct measurements of B_s^0 lifetimes in decays to pure CP eigenstates are available, various experimental results allow for the determination of the lifetimes of the two mass eigenstates. Measurements sensitive to these lifetimes are the angular analysis of $B_s^0 \rightarrow J/\psi\phi$ decays and the branching fraction of $B_s^0 \rightarrow D_s^{(*)+}D_s^{(*)-}$, which can be complemented by measurements of the B_s^0 lifetime in flavor specific final states. The combination of available measurements yields $\tau_s^H = (1.544 \pm 0.041)$ ps and $\tau_s^L = (1.407_{-0.026}^{+0.028})$ ps [14]. From CDF measurements we can infer the two lifetimes from the result of the angular analysis of $B_s^0 \rightarrow J/\psi\phi$ decays. The latest preliminary result [12], that is not yet included in the above average, yields $\tau_s^H = (1.622 \pm 0.068)$ ps and $\tau_s^L = (1.446 \pm 0.035)$ ps assuming standard model CP violation.

Compared to measurements using $B_s^0 \rightarrow J/\psi\phi$ decays, lifetime and future CP violation measurements in the $B_s^0 \rightarrow J/\psi f_0$ decay suffer from a lower branching fraction. Based on a comparison to D_s^+ meson decays Ref. [9] makes a prediction for the branching fraction of $B_s^0 \rightarrow J/\psi f_0$ decay relative to the $B_s^0 \rightarrow J/\psi\phi$ decay,

$$R_{f_0/\phi} = \frac{\mathcal{B}(B_s^0 \rightarrow J/\psi f_0)}{\mathcal{B}(B_s^0 \rightarrow J/\psi\phi)} \frac{\mathcal{B}(f_0 \rightarrow \pi^+\pi^-)}{\mathcal{B}(\phi \rightarrow K^+K^-)}, \quad (7)$$

to be approximately 0.2. The CLEO experiment estimates $R_{f_0/\phi} = 0.42 \pm 0.11$ from a measurement of semileptonic D_s^+ decays [15]. A theoretical prediction based on QCD factorization yields a range of $R_{f_0/\phi}$ between 0.2 and 0.5 [16]. With the world average branching fraction for the $B_s^0 \rightarrow J/\psi\phi$ decay of $(1.3 \pm 0.4) \times 10^{-3}$

and the branching fraction of $f_0 \rightarrow \pi^+\pi^-$ in the region between 0.5–0.8, predictions of $\mathcal{B}(B_s^0 \rightarrow J/\psi f_0)$ [17, 18] translate into a wide range of $R_{f_0/\phi}$ values of approximately 0.1–0.5.

The first experimental search was performed by the Belle experiment [19]. Their preliminary result did not yield a signal and they extract an upper limit on the branching fraction of $\mathcal{B}(B_s^0 \rightarrow J/\psi f_0)\mathcal{B}(f_0 \rightarrow \pi^+\pi^-) < 1.63 \times 10^{-4}$ at 90% C.L. Recently the LHCb experiment reported the first observation of the decay $B_s^0 \rightarrow J/\psi f_0$ [20] with a relative branching fraction of $R_{f_0/\phi} = 0.252^{+0.046}_{-0.032}(\text{stat})^{+0.027}_{-0.033}(\text{syst})$. Shortly after the LHCb result was presented, the Belle collaboration announced their result of an updated analysis using 121.4 fb⁻¹ of $\Upsilon(5S)$ data [21]. They observe a significant $B_s^0 \rightarrow J/\psi f_0$ signal and measure $\mathcal{B}(B_s^0 \rightarrow J/\psi f_0)\mathcal{B}(f_0 \rightarrow \pi^+\pi^-) = (1.16^{+0.31}_{-0.19}{}^{+0.15}_{-0.17}{}^{+0.26}_{-0.18}) \times 10^{-4}$, where the first uncertainty is statistical, the second systematic, and the third one is an uncertainty on the number of produced $B_s^{(*)0}\bar{B}_s^{(*)0}$ pairs. Using their preliminary measurement of the $B_s^0 \rightarrow J/\psi\phi$ branching fraction [22], and assuming that the uncertainty on the number of produced $B_s^{(*)0}\bar{B}_s^{(*)0}$ pairs is fully correlated for the two measurements, this translates into $R_{f_0/\phi} = 0.206^{+0.055}_{-0.034}(\text{stat}) \pm 0.052(\text{syst})$. A preliminary measurement of the D0 experiment yields $R_{f_0/\phi} = 0.210 \pm 0.032(\text{stat}) \pm 0.036(\text{syst})$ [23].

In this paper we present a measurement of the ratio $R_{f_0/\phi}$ of the branching fraction of the $B_s^0 \rightarrow J/\psi f_0$ decay relative to the $B_s^0 \rightarrow J/\psi\phi$ decay and the first measurement of the B_s^0 lifetime in a decay to a pure CP eigenstate. We use data collected by the CDF II detector from February 2002 until October 2008. The data correspond to an integrated luminosity of 3.8 fb⁻¹.

This paper is organized as follows: In Sec. II we describe the CDF II detector together with the online data selection, followed by the candidate selection in Sec. III. Section IV describes details of the measurement of the ratio $R_{f_0/\phi}$ of branching fractions of the $B_s^0 \rightarrow J/\psi f_0$ decay relative to the $B_s^0 \rightarrow J/\psi\phi$ decay while Sec. V discusses the lifetime measurement. We finish with a short discussion of the results and conclusions in Sec. VI.

II. CDF II DETECTOR AND TRIGGER

Among the components of the CDF II detector [24] the tracking and muon detection systems are most relevant for this analysis. The tracking system lies within a uniform, axial magnetic field of 1.4 T strength. The inner tracking volume hosts 7 layers of double-sided silicon micro-strip detectors up to a radius of 28 cm [25]. An additional layer of single-sided silicon is mounted directly on the beam-pipe at a radius of 1.5 cm, providing an excellent resolution of the impact parameter d_0 , defined as the distance of closest approach of the track to the interaction point in the transverse plane. The silicon tracker provides a pseudorapidity coverage up to

$|\eta| \leq 2.0$. The remainder of the tracking volume up to a radius of 137 cm is occupied by an open-cell drift chamber [26]. The drift chamber provides up to 96 measurements along the track with half of them being axial and other half stereo. Tracks with $|\eta| \leq 1.0$ pass the full radial extent of the drift chamber. The integrated tracking system achieves a transverse momentum resolution of $\sigma(p_T)/p_T^2 \approx 0.07\%$ (GeV/c)⁻¹ and an impact parameter resolution of $\sigma(d_0) \approx 35 \mu\text{m}$ for tracks with a transverse momentum greater than 2 GeV/c. The tracking system is surrounded by electromagnetic and hadronic calorimeters, which cover the full pseudorapidity range of the tracking system [27–30]. We detect muons in three sets of multi-wire drift chambers. The central muon detector has a pseudorapidity coverage of $|\eta| < 0.6$ [31] and the calorimeters in front of it provide about 5.5 interaction lengths of material. The minimum transverse momentum to reach this set of muon chambers is about 1.4 GeV/c. The second set of chambers covers the same range in η , but is located behind an additional 60 cm of steel absorber, which corresponds to about 3 interaction lengths. It has a higher transverse momentum threshold of 2 GeV/c, but provides a cleaner muon identification. The third set of muon detectors extends the coverage to a region of $0.6 < |\eta| < 1.0$ and is shielded by about 6 interaction lengths of material.

A three-level trigger system is used for the online event selection. The trigger component most important for this analysis is the extremely fast tracker (XFT) [32], which at the first level groups hits from the drift chamber into tracks in the plane transverse to the beamline. Candidate events containing $J/\psi \rightarrow \mu^+\mu^-$ decays are selected by a dimuon trigger [24] which requires two tracks of opposite charge found by the XFT that match to track segments in the muon chambers and have a dimuon invariant mass in the range 2.7 to 4.0 GeV/c².

III. RECONSTRUCTION AND CANDIDATE SELECTION

A. Reconstruction

In the offline reconstruction we first combine two muon candidates of opposite charge to form a J/ψ candidate. We consider all tracks that can be matched to a track segment in the muon detectors as muon candidates. The J/ψ candidate is subject to a kinematic fit with a vertex constraint. We then combine the J/ψ candidate with two other oppositely charged tracks that are assumed to be pions and have an invariant mass between 0.85 and 1.2 GeV/c² to form a $B_s^0 \rightarrow J/\psi f_0$ candidate. In the final step a kinematic fit of the $B_s^0 \rightarrow J/\psi f_0$ candidate is performed. In this fit we constrain all four tracks to originate from a common vertex, and the two muons forming the J/ψ are constrained to have an invariant mass equal to the world average J/ψ mass [13]. In a similar way we also reconstruct $B_s^0 \rightarrow J/\psi\phi$ candidates using pairs of tracks

of opposite charge assumed to be kaons and having an invariant mass between 1.009 and 1.029 GeV/ c^2 . During the reconstruction we place minimal requirements on the track quality, the quality of the kinematic fit, and the transverse momentum of the B_s^0 candidate to ensure high quality measurements of properties for each candidate. For the branching fraction measurement we add a requirement which aims at removing a large fraction of short-lived background. We require the decay time of the B_s^0 candidate in its own rest frame, the proper decay time, to be larger than three times its uncertainty. This criterion is not imposed in the lifetime analysis since it would bias the lifetime distribution. The proper decay time is determined by the expression

$$t = \frac{L_{xy} \cdot m(B_s^0)}{c \cdot p_T} \quad (8)$$

where L_{xy} is the flight distance projected onto the B_s^0 momentum in the plane transverse to the beamline, p_T is the transverse momentum of the given candidate, and $m(B_s^0)$ is the reconstructed mass of the B_s^0 candidate. The uncertainty on the proper decay time t is estimated for each candidate by propagating track parameter and primary vertex uncertainties into an uncertainty on L_{xy} . The proper decay time resolution is typically of the order of 0.1 ps.

B. Selection

The selection is performed using a neural network based on the NEUROBAYES package [33, 34]. The neural network combines several input variables to form a single output variable on which the selection is performed. The transformation from the multidimensional space of input variables to the single output variable is chosen during a training phase such that it maximizes the separation between signal and background distributions. For each of the two measurements presented in this paper we use a specialized neural network. For the training we need two sets of events with a known classification of signal or background. For the signal sample we use simulated events. We generate the kinematic distributions of B_s^0 mesons according to the measured b -hadron momentum distribution. The decay of the generated B_s^0 particles into the $J/\psi f_0$ final state is simulated using the EVTGEN package [35]. Each event is passed through the standard CDF II detector simulation, based on the GEANT3 package [36, 37]. The simulated events are reconstructed with the same reconstruction software as real data events. The background sample is taken from data using candidates with the $J/\psi \pi^+ \pi^-$ invariant mass above the B_s^0 signal peak, where only combinatorial background events contribute. Because the requirement on the proper decay time significance efficiently suppresses background events in the branching ratio measurement, we use an enlarged sideband region of 5.45 to 5.55 GeV/ c^2 in this analysis,

compared to an invariant mass range from 5.45 to 5.475 GeV/ c^2 for the lifetime measurement.

For the branching fraction measurement, the inputs to the neural network, ordered by the importance of their contribution to the discrimination power, are the transverse momentum of the f_0 , the χ^2 of the kinematic fit of the B_s^0 candidate using information in the plane transverse to the beamline, the proper decay time of the B_s^0 candidate, the quality of the kinematic fit of the B_s^0 candidate, the helicity angle of the positive pion, the transverse momentum of the B_s^0 candidate, the quality of the kinematic fit of the two pions with a common vertex constraint, the helicity angle of the positive muon, and the quality of the kinematic fit of the two muons with common vertex constraint. The helicity angle of the muon (pion) is defined as the angle between the three momenta of the muon (pion) and B_s^0 candidate measured in the rest frame of the J/ψ (f_0). For the selection of $B_s^0 \rightarrow J/\psi \phi$ decays we use the same neural network without retraining and simply replace f_0 variables by ϕ variables and pions by kaons.

For the lifetime measurement we modify the list of inputs by removing the proper decay time. We also do not use the helicity angles as they provide almost no additional separation power on the selected sample. Since we are not concerned about a precise efficiency determination for the lifetime measurement, we add the following inputs: the invariant mass of the two pions, the likelihood based identification information for muons [38], and the invariant mass of the muon pair. The muon identification is based on the matching of tracks from the tracking system to track segments in the muon system, energy deposition in the electromagnetic and hadronic calorimeters, and isolation of the track. The isolation is defined as the transverse momentum carried by the muon candidate over the scalar sum of transverse momenta of all tracks in a cone of $\Delta R = \sqrt{(\Delta\phi)^2 + (\Delta\eta)^2} < 0.4$, where $\Delta\phi$ ($\Delta\eta$) is the difference in azimuthal angle (pseudorapidity) of the muon candidate and the track. There is no significant change in the importance ordering of the inputs. The invariant mass of the pion pair becomes the second most important input, the likelihood based identification of the two muon candidates is ranked fourth and sixth in the importance list, and the muon pair invariant mass is the least important input.

For the branching fraction measurement we select the threshold on the neural network output by maximizing $\epsilon/(2.5 + \sqrt{N_b})$ [39], where ϵ is the reconstruction efficiency for $B_s^0 \rightarrow J/\psi f_0$ decays and N_b is the number of background events estimated from the $J/\psi \pi^+ \pi^-$ mass sideband. The invariant mass distributions of selected $B_s^0 \rightarrow J/\psi f_0$ and $B_s^0 \rightarrow J/\psi \phi$ candidates are shown in Figs. 1 and 2. A clear signal at around 5.36 GeV/ c^2 is visible in both mass distributions.

For the lifetime measurement we use simulated experiments to determine the optimal neural network output requirement. We select a value that minimizes the statistical uncertainty of the measured lifetime. We scan

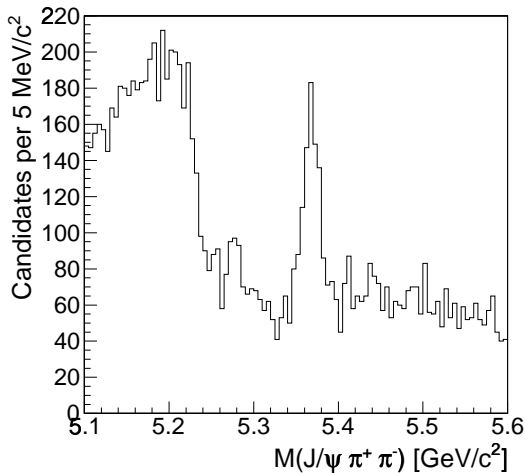


FIG. 1: The invariant mass distribution of $B_s^0 \rightarrow J/\psi f_0$ candidates selected for the branching fraction measurement.

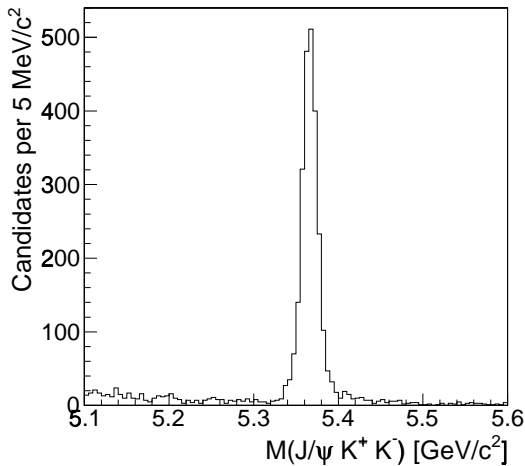


FIG. 2: The invariant mass distribution of $B_s^0 \rightarrow J/\psi \phi$ candidates selected for the branching fraction measurement.

a wide range of neural network output values and for each requirement we simulate an ensemble of experiments with a B_s^0 lifetime of 1.63 ps, where the number of signal and background events as well as the background distributions are simulated according to data. For a broad range of selection requirements we observe the same uncertainty within a few percent. Our final requirement on the network output is chosen from the central region of this broad range of equivalent options.

C. Physics backgrounds

We study possible physics backgrounds using simulated events with all b -hadrons produced and decayed inclusively to final states containing a J/ψ . For this study

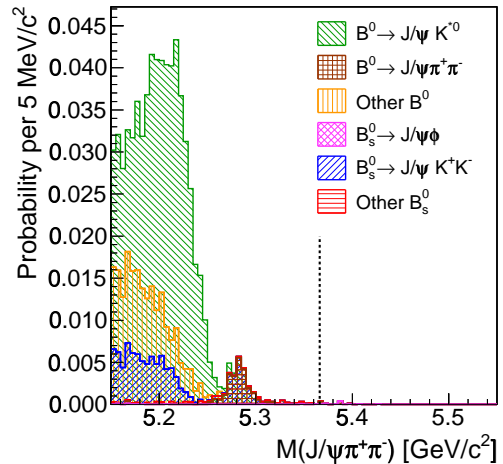


FIG. 3: (color online) Stacked histogram of physics backgrounds derived from simulation using the selection for the branching fraction measurement. The vertical line indicates the location of the world average B_s^0 mass.

we use the selection from the branching fraction measurement. While several physics backgrounds appear in the $J/\psi \pi^+ \pi^-$ mass spectrum, none contributes significantly under the B_s^0 peak. The most prominent physics backgrounds are $B^0 \rightarrow J/\psi K^{*0}$ with $K^{*0} \rightarrow K^+ \pi^-$, where K^{*0} stands for $K^{*0}(892)$, and $B^0 \rightarrow J/\psi \pi^+ \pi^-$. In the first case the kaon is mis-reconstructed as a pion and gives rise to a large fraction of the structure seen below $5.22 \text{ GeV}/c^2$, while the second one is correctly reconstructed and produces the narrow peak at approximately $5.28 \text{ GeV}/c^2$. The stacked histogram of physics backgrounds derived from simulation is shown in Fig. 3. From this study we conclude that the main physics background that has to be included as a separate component in a fit to the mass spectrum stems from decays of $B^0 \rightarrow J/\psi \pi^+ \pi^-$. It is properly reconstructed and therefore simple to parametrize.

IV. BRANCHING FRACTION MEASUREMENT

In this Section we describe details of the branching fraction measurement. These involve the maximum likelihood fit to extract the number of signal events, the efficiency estimation, and the systematic uncertainties. We conclude this Section with the result for the ratio $R_{f_0/\phi}$ of branching fractions between $B_s^0 \rightarrow J/\psi f_0$ and $B_s^0 \rightarrow J/\psi \phi$ decays.

A. Fit description

We use an unbinned extended maximum likelihood fit of the invariant mass to extract the number of B_s^0 decays in our samples. In order to avoid the need for modeling

most of the physics background, we restrict the fit to the mass range from $5.26 \text{ GeV}/c^2$ to $5.5 \text{ GeV}/c^2$. The likelihood is

$$\mathcal{L} = \prod_{i=1}^N [N_s \cdot P_s(m_i) + N_{cb} \cdot P_{cb}(m_i) + f_{pb} \cdot N_s \cdot P_{pb}(m_i) + N_{B^0} \cdot P_{B^0}(m_i)] \cdot e^{-(N_s + N_{cb} + N_s \cdot f_{pb} + N_{B^0})}, \quad (9)$$

where m_i is the invariant mass of the i -th candidate and N is the total number of candidates in the sample. The fit components are denoted by the subscripts s for signal, cb for combinatorial background, pb for physics background, and B^0 for $B^0 \rightarrow J/\psi\pi^+\pi^-$ background. The yields of the components are given by N_s , N_{cb} , $N_s \cdot f_{pb}$, and N_{B^0} , and their probability density functions (PDFs) by $P_{s,cb,pb,B^0}(m_i)$, respectively.

The signal PDF $P_s(m_i)$ is parametrized by a sum of two Gaussian functions with a common mean. The relative size of the two Gaussians and their widths are determined from simulated events. Approximately 82% of the $B_s^0 \rightarrow J/\psi f_0$ decays are contained in a narrower Gaussian with width of $9.4 \text{ MeV}/c^2$. The broader Gaussian has width of $18.4 \text{ MeV}/c^2$. In the case of $B_s^0 \rightarrow J/\psi\phi$, the narrow Gaussian with a width of $7.2 \text{ MeV}/c^2$ accounts for 79% of the signal, with the rest of the events having a width of $13.3 \text{ MeV}/c^2$. To take into account possible differences between simulation and data, we multiply all widths by a single scaling parameter S_m . In the fits all parameters of the PDF are fixed except for the scaling parameter S_m . In addition the mean of the Gaussians is allowed to float in the $J/\psi K^+K^-$ fit. Doing so we obtain a value that is consistent with the world average B_s^0 mass [13]. For the $J/\psi\pi^+\pi^-$ fit we fix the position of the signal to the value determined in the fit to the $J/\psi K^+K^-$ candidates.

The combinatorial background PDF $P_{cb}(m_i)$ is parametrized using a linear function. In both fits we leave its slope floating. In each of the two fits there is one physics background. In the case of the $J/\psi\pi^+\pi^-$ spectrum, the physics background describes properly reconstructed $B^0 \rightarrow J/\psi\pi^+\pi^-$ decays using a shape identical to the B_s^0 signal and position fixed to the world average B^0 mass [13]. The number of B^0 events N_{B^0} is left free in the fit. For the $J/\psi K^+K^-$ fit, we have a contribution from $B^0 \rightarrow J/\psi K^{*0}$ decays where the pion from the K^{*0} decay is mis-reconstructed as a kaon. This contribution peaks at a mass of approximately $5.36 \text{ GeV}/c^2$ with an asymmetric tail towards larger masses. The shape itself is parametrized by a sum of a Gaussian function and an exponential function convolved with a Gaussian. The parameters are derived from simulated $B^0 \rightarrow J/\psi K^{*0}$ events. The normalization of this component relative to the signal is fixed to $(3.04 \pm 0.99) \times 10^{-2}$, which is derived from the CDF Run I measurement of the ratio of cross section times branching fraction for $B_s^0 \rightarrow J/\psi\phi$ and $B^0 \rightarrow J/\psi K^{*0}$ decays [40], the world average branching

fractions for ϕ and K^{*0} [13], and the ratio of reconstruction efficiencies obtained from simulation.

The fit determines a yield of $502 \pm 37 B_s^0 \rightarrow J/\psi f_0$ events and $2302 \pm 49 B_s^0 \rightarrow J/\psi\phi$ events, where the uncertainties are statistical only. The number of B^0 background events in the $J/\psi\pi^+\pi^-$ fit is 160 ± 30 .

B. Efficiency

To extract the ratio of branching fractions we need to estimate the relative efficiency for reconstruction of $B_s^0 \rightarrow J/\psi f_0$ with $f_0 \rightarrow \pi^+\pi^-$ and $B_s^0 \rightarrow J/\psi\phi$ with $\phi \rightarrow K^+K^-$ decays, $\epsilon_{rel} = \epsilon(B_s^0 \rightarrow J/\psi\phi)/\epsilon(B_s^0 \rightarrow J/\psi f_0)$. We estimate the efficiency using simulated events in which we generate a single B_s^0 meson per event. The B_s^0 meson then decays with equal probabilities to $B_s^0 \rightarrow J/\psi f_0$ or $B_s^0 \rightarrow J/\psi\phi$ final states with exclusive $J/\psi \rightarrow \mu^+\mu^-$, $\phi \rightarrow K^+K^-$, and $f_0 \rightarrow \pi^+\pi^-$. Generated events are then processed through a detailed detector simulation and the offline reconstruction software used to reconstruct data. In both cases angular and decay time distributions are generated assuming no CP violation and parameters taken from the preliminary result of the angular distributions analysis [12]: $\tau = 1.529 \pm 0.028 \text{ ps}$, $\Delta\Gamma = 0.075 \pm 0.036 \text{ ps}^{-1}$, $|A_0|^2 = 0.524 \pm 0.020$, and $|A_{||}|^2 = 0.231 \pm 0.021$. As a strong phase between A_0 and $A_{||}$ is not measured we use the world average value from $B^0 \rightarrow J/\psi K^{*0}$ decays of $\phi_{||} = -2.86 \pm 0.11$ [13] as a reasonable approximation [41]. An additional peculiarity of the $B_s^0 \rightarrow J/\psi f_0$ decay is the unusual mass shape of the f_0 meson. It is modeled using a Flatté distribution [42] with input parameters measured by the BES experiment [43] to be $m_0 = 965 \pm 8 \pm 6 \text{ MeV}/c^2$, $g_\pi = 165 \pm 10 \pm 15 \text{ MeV}/c^2$, and $g_K/g_\pi = 4.21 \pm 0.25 \pm 0.21$, where the errors are statistical and systematic, respectively. The ϕ meson mass distribution is modeled using a relativistic Breit-Wigner distribution with world average values for its parameters [13]. With these inputs to the simulation we find $\epsilon_{rel} = 1.178$, which accounts for the ϕ and f_0 mass window selection requirements.

C. Systematic uncertainties

We investigate several sources of systematic uncertainties. They can be broadly separated into two classes: one dealing with assumptions made in the fits that may affect yields, and the other related to assumptions in the efficiency estimation. In the first class we estimate uncertainties by refitting data with a modified assumption and taking the difference with respect to the original value as an uncertainty. For the second class we recalculate the efficiency with a modified assumption and take the difference with respect to the default efficiency as an uncertainty unless specified otherwise. The summary of assigned uncertainties is given in Table I.

For the yield of $B_s^0 \rightarrow J/\psi\phi$ we investigate the effect of the assumption on the combinatorial background shape, the limited knowledge of mis-reconstructed $B^0 \rightarrow J/\psi K^{*0}$ decays and the shape of the signal PDF. The uncertainty due to the shape of combinatorial background is estimated by changing from the first order polynomial to a constant or a second order polynomial. For the physics background we vary the normalization of the component in the fit and use an alternative shape determined by varying the momentum distribution and the decay amplitudes of $B^0 \rightarrow J/\psi K^{*0}$ in simulation. Finally, to estimate the effect of the signal PDF parametrization we use an alternative model with a single Gaussian rather than two Gaussian functions and an alternative shape from simulation, where we vary the momentum distribution of the produced B_s^0 mesons and the decay amplitudes of the $B_s^0 \rightarrow J/\psi\phi$ decay.

To estimate the uncertainty on the $B_s^0 \rightarrow J/\psi f_0$ yield we follow a procedure similar to that for $B_s^0 \rightarrow J/\psi\phi$ and conservatively treat the systematic effects as independent between the two modes in the calculation of $R_{f_0/\phi}$. For the sensitivity to the parametrization of the combinatorial background we switch to a second order polynomial or a constant as alternative parametrization. For the shape of the signal PDF we use two alternatives, one with a single Gaussian function instead of two and another one with two Gaussians, but varying the momentum distribution in simulation. We also vary the position of the B_s^0 signal within the uncertainty determined in the $J/\psi K^+ K^-$ fit.

The systematic uncertainty on the relative efficiency stems from the statistics of simulation, an imperfect knowledge of the momentum distribution, physics parameters of decays like lifetimes or decay amplitudes, and differences in the efficiencies of the online selection of events. To estimate the effect of the imperfect knowledge of the momentum distribution we vary the momentum distribution of B_s^0 mesons in the simulation. The physics parameters entering the simulation are grouped into three categories, those defining the f_0 mass shape, the ones determining decay amplitudes in $B_s^0 \rightarrow J/\psi\phi$ decays, and those affecting the lifetimes of the two B_s^0 mass eigenstates. In the first two cases we vary each parameter independently and add all changes in the efficiency in quadrature. For the last case we vary the mean lifetime τ and the decay width difference $\Delta\Gamma$ simultaneously and take the largest variation as the uncertainty. We add the uncertainty from the third class in quadrature with all others to obtain the uncertainty due to the parameters describing the particle decays. The last effect deals with how events are selected during data taking. The CDF trigger has several different sets of requirements for the selection of events. The ones used in this analysis can be broadly sorted into three classes depending on momentum thresholds and which subdetectors detected muons. The fraction of events for each different class varies depending on the instantaneous luminosity, which is not simulated. To estimate the size of a possible effect we

TABLE I: The summary of assigned systematic uncertainties for the branching fraction measurement.

Source	$J/\psi\phi$ yield	$J/\psi f_0$ yield	ϵ_{rel}
Combinatorial bckg.	34	16	–
Physics bckg.	13	–	–
Mass resolution	32	7.9	–
B_s^0 mass	–	0.1	–
Total	49	18	–
MC statistics	–	–	0.012
Momentum distribution	–	–	0.011
Decay parameters	–	–	0.033
Trigger composition	–	–	0.016
Total	–	–	0.040

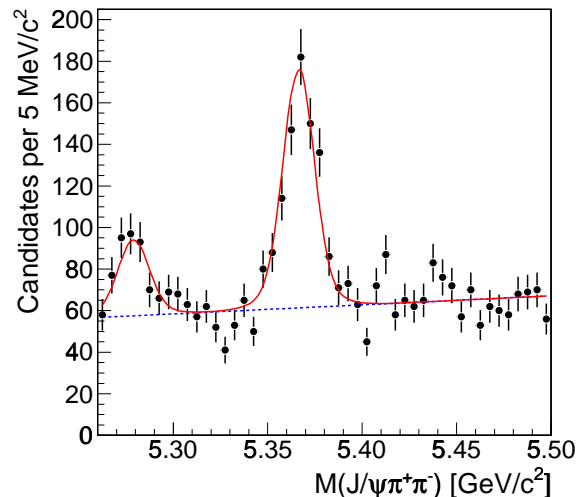


FIG. 4: (color online) Projection of the fit of the $B_s^0 \rightarrow J/\psi f_0$ decay mode. The dashed line (blue) shows the contribution from combinatorial background.

calculate the efficiency for each class separately and take half of the largest difference as the uncertainty.

To obtain the total uncertainty we add all partial uncertainties in quadrature. In total we assigned 49 events (2.1%) as the systematic uncertainty on the $B_s^0 \rightarrow J/\psi\phi$ yield, 18 events (3.6%) on the $B_s^0 \rightarrow J/\psi f_0$ yield, and 0.040 (3.4%) on the relative efficiency ϵ_{rel} . A summary of the systematic uncertainties in the branching ratio is provided in Table I.

D. Branching fraction result

From the fit we find $502 \pm 37(\text{stat}) \pm 18(\text{syst})$ $B_s^0 \rightarrow J/\psi f_0$ signal events and $2302 \pm 49(\text{stat}) \pm 49(\text{syst})$ $B_s^0 \rightarrow J/\psi\phi$ events. The projections of the fits for $B_s^0 \rightarrow J/\psi f_0$ and $B_s^0 \rightarrow J/\psi\phi$ are shown in Fig. 4 and Fig. 5, respectively.

In order to check our interpretation of the signal in the $J/\psi\pi^+\pi^-$ distribution being due to the $B_s^0 \rightarrow J/\psi f_0$

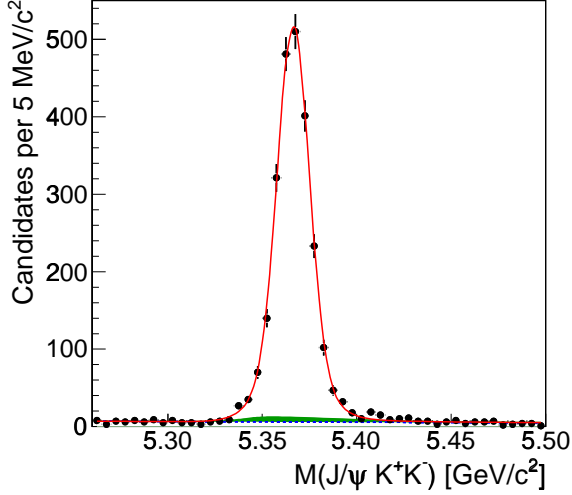


FIG. 5: (color online) Projection of the fit of the $B_s^0 \rightarrow J/\psi\phi$ decay mode. The dashed line (blue) and filled area (green) show the contributions from combinatorial background and $B^0 \rightarrow J/\psi K^{*0}$, respectively.

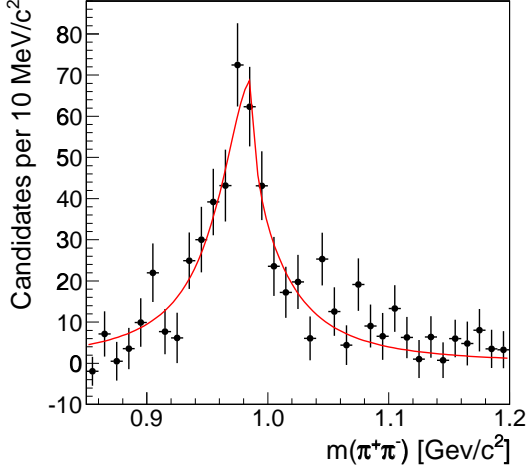


FIG. 6: The dipion invariant mass distribution after sideband subtraction with fit projection overlaid. The fit uses a Flatté distribution with all parameters floating.

decays we show the invariant mass distribution of the pions for B_s^0 signal data in Fig. 6. To obtain the distribution of B_s^0 signal we fit the $J/\psi\pi^+\pi^-$ mass distribution in the range 5.26 to 5.45 GeV/c^2 for each bin in $\pi^+\pi^-$ mass and report the B_s^0 signal yield as a function of $\pi^+\pi^-$ mass. We fit the dipion mass distribution using the Flatté parametrization. The obtained parameters, $m_0 = 989.6 \pm 9.9(\text{stat}) \text{ MeV}/c^2$, $g_\pi = 141 \pm 19(\text{stat}) \text{ MeV}/c^2$, and $g_K/g_\pi = 2.3 \pm 1.3(\text{stat})$, are in reasonable agreement with the ones measured by the BES collaboration [43] with a fit probability of 23.4%. In Figs. 7 and 8 we show the positive muon and pion helicity angle dis-

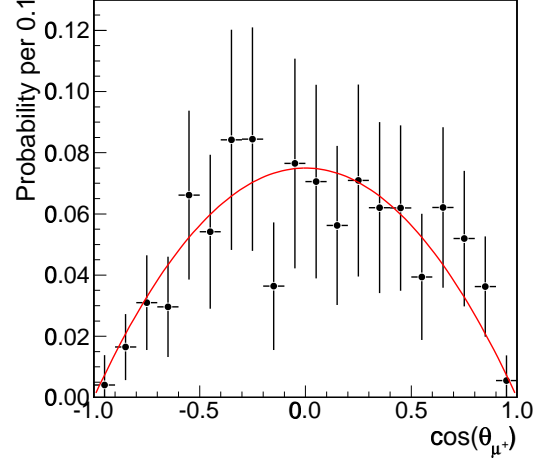


FIG. 7: Normalized helicity angle distribution for the positive muon corrected for relative efficiency. The line shows the expectation for a $B_s^0 \rightarrow J/\psi f_0$ decay.

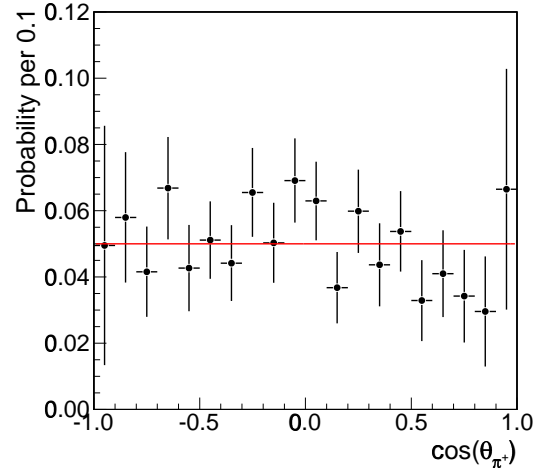


FIG. 8: Normalized helicity angle distribution for the positive pion corrected for relative efficiency. The line shows the expectation for a $B_s^0 \rightarrow J/\psi f_0$ decay.

tributions, obtained in an analogous way to the invariant mass distribution of pion pairs. Those are corrected for relative efficiencies in the different helicity bins and compared to the theoretical expectation for a $B_s^0 \rightarrow J/\psi f_0$ signal. We use a χ^2 test to evaluate the agreement between data and theoretical expectation. For the distribution of $\cos(\theta_{\mu^+})$ we obtain $\chi^2/\text{ndf} = 7.9/20$, which corresponds to 99% probability. Similarly for $\cos(\theta_{\pi^+})$ the χ^2/ndf is 15/20, giving 78% probability. Since the dipion mass as well as the angular distributions are consistent with expectations, we interpret our signal as coming solely from the $B_s^0 \rightarrow J/\psi f_0$ decays. On the other hand, as we use a dipion mass window from 0.85 to 1.2 GeV/c^2 , we cannot exclude contributions from other higher mass

states to our signal with present statistics.

Finally, we obtain the ratio of branching fractions

$$R_{f_0/\phi} = \frac{\mathcal{B}(B_s^0 \rightarrow J/\psi f_0) \mathcal{B}(f_0 \rightarrow \pi^+ \pi^-)}{\mathcal{B}(B_s^0 \rightarrow J/\psi \phi) \mathcal{B}(\phi \rightarrow K^+ K^-)} = 0.257 \pm 0.020(\text{stat}) \pm 0.014(\text{syst}), \quad (10)$$

where corrections for events with an f_0 or ϕ mass outside the ranges selected in this analysis are taken into account.

V. LIFETIME MEASUREMENT

In this Section we discuss the details of the lifetime measurement. We describe the maximum likelihood fit, estimate the systematic uncertainties, and present the result of the lifetime measurement.

A. Fit description

To extract the B_s^0 lifetime we use a maximum likelihood fit. The fit uses three variables: the invariant mass m_i , the decay time t_i , and the decay time uncertainty σ_{t_i} of each candidate. To exclude $B^0 \rightarrow J/\psi \pi^+ \pi^-$ decays we use only candidates with an invariant mass greater than 5.3 GeV/ c^2 in the fit.

The components in the fit are B_s^0 signal and combinatorial background. The likelihood function has the form

$$\mathcal{L} = \prod_{i=1}^N [f_s \cdot P_s(m_i, t_i, \sigma_{t_i}) + (1 - f_s) \cdot P_{cb}(m_i, t_i, \sigma_{t_i})]. \quad (11)$$

The parameter f_s denotes the fraction of signal $B_s^0 \rightarrow J/\psi f_0$ decays and P_s and P_{cb} the probability density function of signal and combinatorial background, respectively. To enhance the signal-to-background ratio in the selected sample, we use only B_s^0 candidates with decay times larger than 0.2 mm/ $c = 0.67$ ps. This requirement suppresses background by a factor of 40 and reduces the prompt background component to a negligible level while keeping about two thirds of the signal events.

The B_s^0 signal mass PDF is parametrized as for the branching ratio measurement. The PDF in decay time is parametrized with an exponential function convolved with a Gaussian resolution function. The width of the Gaussian is given by the candidate-specific estimated decay time uncertainty σ_{t_i} scaled by a common factor S_t which accounts for possible discrepancies between estimated and actual resolutions. The scaling factor S_t is determined in a fit to data dominated by prompt background, selected by requiring $t < 0.3$ ps. In the final fit, S_t is a free parameter with a Gaussian constraint applied. The PDF in decay time uncertainty is parametrized by an empirical function. We use a log-normal distribution

with parameters μ , θ , and σ defined as

$$\mathcal{D}(\sigma_{t_i} | \mu, \theta, \sigma) = \frac{1}{\sqrt{2\pi}\sigma(\sigma_{t_i} - \mu)} \cdot e^{-\frac{(\ln(\sigma_{t_i} - \mu) - \theta)^2}{2\sigma^2}} \quad (12)$$

for $\sigma_{t_i} > \mu$ and zero otherwise. Given the rather small statistics of the B_s^0 signal we derive the parameters using simulated $B_s^0 \rightarrow J/\psi f_0$ events and Gaussian constrain the values in the fit to data.

The mass PDF for combinatorial background is parametrized by a linear function. The decay time PDF for the combinatorial background is composed of two parts, each described by an exponential convolved with the same resolution function as used for signal. The long-lived part accounts for the background from b -hadron decays and the short-lived part describes the tail from mis-reconstructed prompt events. The decay time uncertainty PDFs are again modeled using log-normal distributions, one for the long-lived background component and one for the short-lived component. The parameters of each log normal distribution are independent of the distribution of the B_s^0 signal.

All parameters of the combinatorial background are determined from the fit. The yield, the mass resolution scale factor, and the lifetime of the B_s^0 signal are also left to float freely. The decay time uncertainty parameters of the signal and the resolution scale parameter are Gaussian constrained. Using an ensemble of simulated experiments we verify within 1% that the fit is unbiased and returns proper uncertainties.

B. Systematic uncertainties

We investigate several possible sources of systematic uncertainties. These are broadly separable into two classes: the first dealing with the parametrization of the PDFs and the second with possible biases in the selection or reconstruction.

We first investigate our assumption of the mass shape of combinatorial background. We determine the relative change of the B_s^0 lifetime between a fit with a first and a third order polynomial background mass model for different invariant mass ranges. We find an average relative difference of 0.010 ps, which we assign as the systematic uncertainty. The systematic uncertainty assigned to the signal mass shape has contributions from the limited knowledge of the mean position and from the assumed shape parametrization. Both effects are evaluated in the same way as for the branching ratio measurement and yield a systematic uncertainty of 0.005 ps. There are two assumptions made for the decay time PDFs; one is the resolution scale factor, S_t , which is known only with limited precision and the other is the shape of the combinatorial background. The uncertainty of the scale S_t is included directly in the statistical uncertainty of the fit as the parameter is allowed to vary within a Gaussian constraint. To quantify the size of the contribution, we repeat the fit with S_t fixed to its central value and find

TABLE II: Summary of assigned systematic uncertainties for the lifetime measurement. The uncertainties in parentheses are included in the statistical uncertainty via Gaussian constraints in the fit.

Source	Uncertainty [ps]
Background mass model	0.010
Signal mass model	0.005
Decay time uncertainty scale	(< 0.01)
Background decay time model	0.021
Decay time uncertainty model	(0.015)
SVX alignment	0.007
Total	0.03

the quadratic difference in uncertainty to the original fit to be well below 0.01 ps. To estimate the effect of the assumed decay time PDF of combinatorial background, we employ an alternative fit method which does not need a decay time parametrization of the background. We split the data into several decay time bins and simultaneously fit the invariant mass distributions with independent parameters for the background in each bin. The signal yield is determined by integrating the signal decay time PDF over each bin. Comparing the fit results of the two methods for different selection requirements we find an average relative difference of 0.021 ps which is assigned as systematic uncertainty. The third kind of systematic effect addresses the uncertainty of the σ_t PDFs. The main effect is the distribution for signal derived from simulated events. The uncertainty is already included in the statistical error since the parameters are Gaussian constrained in the fit. The widths of the Gaussian constraints are chosen to cover possible differences between simulation and data. The relative uncertainty due to modeling of the decay time uncertainty distribution, estimated from a comparison of fit results with fixed and constrained parameters, is 0.015 ps.

For the second class, we verify that our candidate selection does not introduce any significant bias. A bias in the mass distribution could artificially enhance or decrease the amount of signal candidates while a bias in decay time could directly affect the extracted lifetime. We verify on a background-enriched sample selected by requiring $t < 0.01$ cm/c that no artificial peak is observed for any neural network output requirement. With a high statistics sample of simulated events we check that the selection does not bias the fitted lifetime. A possible lifetime-bias introduced by the trigger has been studied in a previous CDF analysis [44] and is negligible in our measurement. Finally the alignment of the tracking detectors is known only with finite precision. Previous measurements found that the uncertainty on the lifetime due to a possible misalignment is 0.007 ps [44].

All the contributions are added in quadrature and yield a total systematic error on the lifetime of 0.03 ps (1.5%). A summary of the systematic uncertainties on the lifetime is provided in Table II.

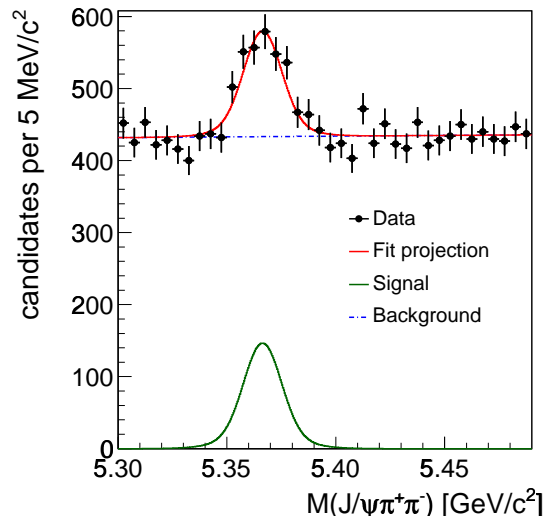


FIG. 9: (color online) Invariant mass distribution with fit projection overlaid.

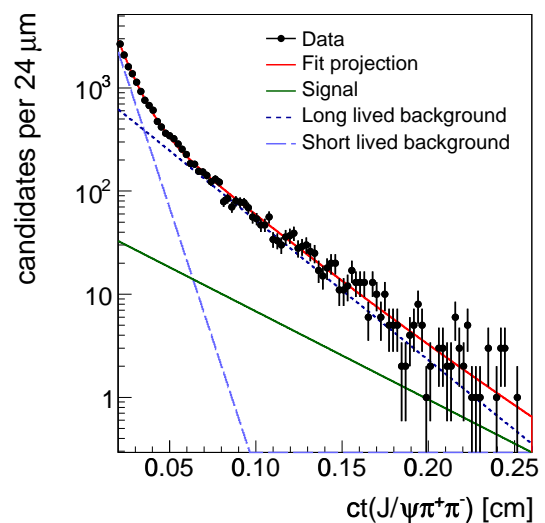


FIG. 10: (color online) Decay time distribution with fit projection overlaid.

C. Lifetime result

Performing the likelihood fit to the selected data we extract the B_s^0 lifetime in $B_s^0 \rightarrow J/\psi f_0$ decays

$$\tau(B_s^0 \rightarrow J/\psi f_0) = 1.70_{-0.11}^{+0.12}(\text{stat}) \pm 0.03(\text{syst}) \text{ ps.} \quad (13)$$

In Figs. 9 to 11 we show the data together with the projection of the fit.

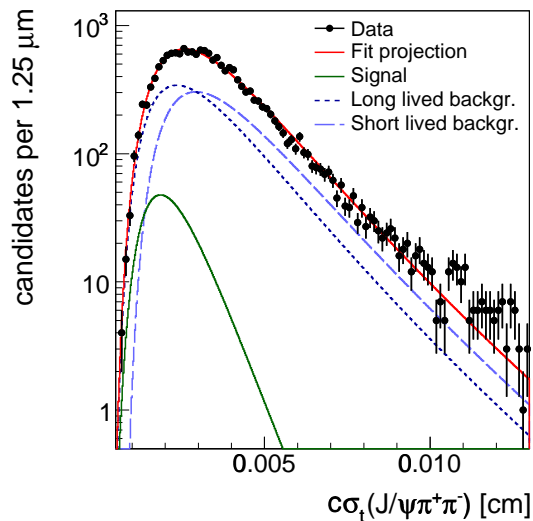


FIG. 11: (color online) Decay time uncertainty distribution with fit projection overlaid.

VI. CONCLUSIONS

We confirm the observation of the $B_s^0 \rightarrow J/\psi f_0(980)$ decay from the LHCb [20] and Belle [21] experiments. The observed signal is the world's largest and we perform the most precise measurement of the ratio of branching fractions $R_{f_0/\phi}$ between $B_s^0 \rightarrow J/\psi f_0$ and $B_s^0 \rightarrow J/\psi \phi(980)$ decays:

$$R_{f_0/\phi} = \frac{\mathcal{B}(B_s^0 \rightarrow J/\psi f_0(980)) \mathcal{B}(f_0(980) \rightarrow \pi^+ \pi^-)}{\mathcal{B}(B_s^0 \rightarrow J/\psi \phi) \mathcal{B}(\phi \rightarrow K^+ K^-)} = 0.257 \pm 0.020(\text{stat}) \pm 0.014(\text{syst}). \quad (14)$$

In this result we assume that the observed signal is solely due to the decay $B_s^0 \rightarrow J/\psi f_0(980)$ and correct for the acceptance of the invariant mass selection of the pion pair. Using the world average $B_s^0 \rightarrow J/\psi \phi$ branching fraction [13] $R_{f_0/\phi}$ can be converted into the product of branching fractions of

$$\mathcal{B}(B_s^0 \rightarrow J/\psi f_0(980)) \mathcal{B}(f_0(980) \rightarrow \pi^+ \pi^-) = (1.63 \pm 0.12 \pm 0.09 \pm 0.50) \times 10^{-4}, \quad (15)$$

where the first uncertainty is statistical, the second is systematic, and the third one is due to the uncertainty on the $B_s^0 \rightarrow J/\psi \phi$ and $\phi \rightarrow K^+ K^-$ branching fractions. The measurement presented here agrees well with the

previous measurements of this quantity and with theoretical predictions.

Moreover, our sample allows us to measure the B_s^0 lifetime in the $B_s^0 \rightarrow J/\psi f_0(980)$ decay mode:

$$\tau(B_s^0 \rightarrow J/\psi f_0(980)) = 1.70_{-0.11}^{+0.12}(\text{stat}) \pm 0.03(\text{syst}) \text{ ps}. \quad (16)$$

This is the first measurement of the B_s^0 lifetime in a decay to a pure CP eigenstate. In the context of the standard model the lifetime measured in this decay mode to a CP -odd final state can be interpreted as the lifetime of the heavy B_s^0 eigenstate. The measured value agrees well both with the standard model expectation as well as with other experimental determinations.

While the precision of the lifetime measurement is still limited by statistics, it provides an important cross-check on the result determined in $B_s^0 \rightarrow J/\psi \phi$ decays, which relies on an angular separation of two CP eigenstates. Furthermore, the measured lifetime can be used as an external constraint in the $B_s^0 \rightarrow J/\psi \phi$ analysis to improve the determination of the CP -violating phase in the $B_s^0 \rightarrow J/\psi \phi$ decay. The lifetime measurement in $B_s^0 \rightarrow J/\psi f_0(980)$ decays is also the next step towards a tagged time dependent CP -violation measurement, which can provide an independent constraint on the CP violation in B_s^0 mixing.

Acknowledgments

We thank the Fermilab staff and the technical staffs of the participating institutions for their vital contributions. This work was supported by the U.S. Department of Energy and National Science Foundation; the Italian Istituto Nazionale di Fisica Nucleare; the Ministry of Education, Culture, Sports, Science and Technology of Japan; the Natural Sciences and Engineering Research Council of Canada; the National Science Council of the Republic of China; the Swiss National Science Foundation; the A.P. Sloan Foundation; the Bundesministerium für Bildung und Forschung, Germany; the Korean World Class University Program, the National Research Foundation of Korea; the Science and Technology Facilities Council and the Royal Society, UK; the Institut National de Physique Nucleaire et Physique des Particules/CNRS; the Russian Foundation for Basic Research; the Ministerio de Ciencia e Innovación, and Programa Consolider-Ingenio 2010, Spain; the Slovak R&D Agency; and the Academy of Finland.

[1] C. Gay, Annu. Rev. Nucl. Part. Sci. **50**, 577 (2000).
 [2] A. Lenz and U. Nierste, J. High Energy Phys. **06**, 072 (2007).
 [3] U. Nierste and A. Lenz, arXiv:hep-ph/1102.4274.

[4] I. Dunietz, R. Fleischer, and U. Nierste, Phys. Rev. D **63**, 114015 (2001).
 [5] A. S. Dighe, I. Dunietz, H. J. Lipkin, and J. L. Rosner, Phys. Lett. B **369**, 144 (1996).

- [6] S. Stone and L. Zhang, arXiv:hep-ex/0909.5442.
- [7] T. Aaltonen *et al.* (CDF Collaboration), Phys. Rev. Lett. **100**, 161802 (2008).
- [8] V. M. Abazov *et al.* (D0 Collaboration), Phys. Rev. Lett. **101**, 241801 (2008).
- [9] S. Stone and L. Zhang, Phys. Rev. D **79**, 074024 (2009).
- [10] S. Stone, arXiv:hep-ph/1009.4939.
- [11] F. Azfar *et al.*, J. High Energy Phys. 1011, 158 (2010).
- [12] T. Aaltonen *et al.* (CDF Collaboration), CDF Public Note 10206, 2010 (unpublished).
- [13] K. Nakamura *et al.* (Particle Data Group), J. Phys. G **37**, 075021 (2010).
- [14] D. Asner *et al.* (Heavy Flavor Averaging Group), arXiv:hep-ex/1010.1589.
- [15] K. Ecklund *et al.* (CLEO Collaboration), Phys. Rev. D **80**, 052009 (2009).
- [16] O. Leitner, J.-P. Dedonder, B. Loiseau, and B. El-Bennich, Phys. Rev. D **82**, 076006 (2010).
- [17] P. Colangelo, F. De Fazio, and W. Wang, Phys. Rev. D **81**, 074001 (2010).
- [18] P. Colangelo, F. De Fazio, and W. Wang, arXiv:hep-ph/1009.4612.
- [19] R. Louvot, arXiv:hep-ex/1009.2605.
- [20] R. Aaij *et al.* (LHCb Collaboration), Phys. Lett. B **698**, 115 (2011).
- [21] J. Li *et al.* (Belle Collaboration), Phys. Rev. Lett. **106**, 121802 (2011).
- [22] R. Louvot, arXiv:hep-ex/0905.4345.
- [23] D0 Collaboration, Conference Note 6152
- [24] D. E. Acosta *et al.* (CDF Collaboration), Phys. Rev. D **71**, 032001 (2005).
- [25] C. S. Hill, Nucl. Instrum. Methods A **530**, 1 (2004).
- [26] A. A. Affolder *et al.*, Nucl. Instrum. Methods A **526**, 249 (2004).
- [27] L. Balka *et al.*, Nucl. Instrum. Methods A **267**, 272 (1988).
- [28] S. Bertolucci *et al.*, Nucl. Instrum. Methods A **267**, 301 (1988).
- [29] M. G. Albrow *et al.*, Nucl. Instrum. Methods A **480**, 524 (2002).
- [30] G. Apollinari, K. A. Goulianos, P. Melese, and M. Lindgren, Nucl. Instrum. Methods A **412**, 515 (1998).
- [31] G. Ascoli *et al.*, Nucl. Instrum. Methods A **268**, 33 (1998).
- [32] E. J. Thomson *et al.*, IEEE Trans. Nucl. Sci., **49**, 1063 (2002).
- [33] M. Feindt and U. Kerzel, Nucl. Instrum. Methods A **559**, 190 (2006).
- [34] M. Feindt, arXiv:physics/0402093.
- [35] D. Lange, Nucl. Instrum. Methods A **462**, 152 (2001).
- [36] R. Brun, R. Hagelberg, M. Hansroul, and J. Lassalle, CERN-DD-78-2-REV, 1978 (unpublished).
- [37] E. Gerchtein and M. Paulini, arXiv:physics/0306031.
- [38] G. Giurgiu, Ph.D. thesis, Carnegie Mellon University, FERMILAB-THESIS-2005-41, 2005.
- [39] G. Punzi, arXiv:physics/0308063.
- [40] F. Abe *et al.* (CDF Collaboration), Phys. Rev. D **54**, 6596 (1996).
- [41] M. Gronau and J. L. Rosner, Phys. Lett. B **669**, 321 (2008).
- [42] S. M. Flatté, Phys. Lett. B **63**, 224 (1976).
- [43] M. Ablikim *et al.* (BES Collaboration), Phys. Lett. B **607**, 243 (2005).
- [44] T. Aaltonen *et al.* (CDF Collaboration), Phys. Rev. Lett. **106**, 121804 (2011).